Electronic Supplementary Information (ESI)

Non-covalent Metalation of Carbon Nitride for Photocatalytic NADH Regeneration and enzymatic CO_2 Reduction

Yuanyuan Zhang,[ab] Xiaonan Kan,[a] Yutai Zou,[a] Jian Liu[ab*]

[a] *College of Materials Science and Engineering, Qingdao University of Science and Technology, Qingdao 266042 (P.R. China).*
[b] *Qingdao Institute of Bioenergy and Bioprocess Technology, Chinese Academy of Sciences, Shandong Energy Institute, Qingdao 266101 (P.R. China)*

*Corresponding Author: liujian@qust.edu.cn

Experimental Section

Materials

Cyanamide solution, nicotinamide adenine dinucleotide hydrate (NAD^+), and formate dehydrogenase from Candida boidinii (FDH, EC.1.2.1.2, F8649) were purchased from Sigma-Aldrich, USA. Silica gel and 2,2'-bipyridine were purchased from Titan Scientific Co., Ltd, Shanghai. Pentamethylcyclopentadienyl rhodium (III) chloride dimer $(Cp^*RhCl_2)_2$ was purchased from Shanghai Aladdin Biochemical Technology Co., Ltd. NaH_2PO_4, Na_2HPO_4 were purchased from Sinopharm Chemical Reagent. All chemicals were used without further purification. Commercial hydrophobic membranes (PLGC, 10 kDa, d = 44.5 mm, Millipore) used in this work were purchased from Merck millipore, USA.

Preparation of the CN samples

Preparation of CN

Multi-porous carbon nitride (CN) was prepared applying cyanamide as precursor following a thermal polymerization process, where silica gels were used as template. In a typical synthesis, 2 g cyanamide solution and 750 mg silica gel were first mixed in methanol with continuous stirring for 2 hours, following which the mixture was dried through rotary evaporation. The obtained powder was then pyrolyzed in a quartz boat at 550 °C under N_2 flow. After calcination for 4 hours, CN was obtained through an etching treatment with 10 wt % HF solution for 12 h to remove the templates.

Preparation of bpy@CN

A post loading method was used to prepare bpy_{mx}@CN. In a typical preparation

process, 25 μmol of 2,2'-bipyridine was dissolved completely in 20 ml of methanol solution. Then 300 mg of CN was added and the mixture was sonicated for a while for the uniform dispersion of CN. After being stirred at room temperature for 3 hours, the bpy_{m1}@CN precursor could be obtained following further drying via rotary evaporation. The precursor powder was then annealed at 200 °C with a heating ramp of 5 °C/min for an hour. After cooling to room temperature, the final product, bpy_{m1}@CN, was received. For comparison, bpy_{m2}@CN, bpy_{m3}@CN, and bpy_{m4}@CN were synthesized through a similar preparation procedure with varying the amount of 2,2'-bipyridine as 75 μmol, 125 μmol, and 350 μmol, respectively.

Preparation of Rh@CN

Rh_{mx}@CN was prepared by coordinating Rh onto the bpy_{mx}@CN accordingly. Taking Rh_{m1}@CN for example, 6.5 μmol $(Cp^*RhCl_2)_2$ was dissolved in 5 ml methanol. Separately, 150 mg bpy_{m1}@CN was dispersed in 15 ml methanol and sonicated for 10 min. After adding bpy_{m1}@CN dispersion into the Rh solution, the mixture was stirred at room temperature for 12 hours. After centrifugation and washing for at least three times with CH_3OH, Rh_{m1}@CN can be obtained upon vacuum drying. Following the same procedure, but setting the $(Cp^*RhCl_2)_2$ amount as 19.5, 32.5, and 90 μmol, respectively. Rh_{m2}@CN, Rh_{m3}@CN, and Rh_{m4}@CN can be obtained finally.

Photocatalytic NADH regeneration

Photocatalytic NADH regeneration was performed in a 3 ml quartz cuvette under ambient condition with continuous irradiation from a 36W LED lamp (λ=450 nm). All the kinetic measurements were conducted with a UV-vis spectrophotometer (U-3900,

HITACHI). In a typical procedure, 3 ml of the total reaction solution containing photocatalyst (9 mg), NAD^+ (1 mM), phosphate buffer solution (PBS) (pH = 7.4, 100 mM) was added into a quartz bottle. The dispersion was first stirred in darkness for 10 minutes to reach adsorption-desorption equilibrium prior to the irradiation. Then, it was illuminated with the LED light. Sample aliquot was taken in regular time intervals, and the concentration of NADH was measured from the absorbance at 340 nm using a UV-vis spectrometer. Catalytic conversion was calculated using the formula bellow:

NADH conversion (%) = $[(A_1-A_0) \times \text{dilution ratio}]/6.22 \times 100\%$

where A_0 and A_1 refer to the initial and final absorbance values at 340 nm, respectively. The constant 6.22 results from the absorption coefficient (6220 M^{-1} cm^{-1}) of the absorption peak at 340 nm.

For the reusability test, photocatalysts after catalytic reactions were washed with DI water, and was then collected through centrifugation before reuse.

Photoelectrochemical measurements

Photoelectrochemical measurements were conducted on a CHI660 electrochemical workstation using a standard three-electrode single-cell compartment. 0.2 M Na_2SO_4, Pt foil, and Ag/AgCl were used as the electrolyte, counter electrode, and reference electrode, respectively. The working electrodes were prepared by dispersing the ethanol/Nafion solution containing 10 mg ml^{-1} catalysts on fluorine-doped tin oxide (FTO) glasses with target area of 1 cm × 1 cm. After drying at room temperature, the electrodes were heated at 60 °C for 1 hour to improve adhesion. The electrochemical impedance spectroscopy (EIS) measurement and photocurrent response

measurement were performed without bias voltage.

FDH immobilization

The “fouling-induced immobilization” method was applied to load enzyme on the hydrophobic membrane using a filtration cell (Amicon 8050, Millipore, USA). Before immobilization, the membrane was pre-soaked in 5% NaCl solution for 30 min and then filtered with DI water for another 30 min at 1 bar (procedures according to the manufacturers’ instructions) after leaching with water thoroughly. For immobilization, 6 mg FDH was first dissolved in 25 ml PBS to get the enzyme solution. Then place the membrane at the bottom of the cell, below which there is already an extra ordinary membrane and make sure the hydrophobic side of the membrane facing the enzyme solution. After that, pour the enzyme solution into the cell and filtrate at a pressure of 2 bar. At last, wash the obtained biomembrane with 20 ml PBS at a pressure of 2 bar, and rinsed 3 times with PBS without pressure.

Photo-enzyme coupled HCOOH production from CO_2

The photoenzymatic production of HCOOH from CO_2 was performed in a 3 ml quartz cuvette under ambient condition with continuous irradiation from a 36W LED lamp (λ=450 nm). Typically, the system contains 2.88 ml PBS, 9 mg photocatalyst, 120 μl NAD^+, and 1 unit FDH. It is worth noting that the FDH in the system exists either in a dissociative form or in the form of fixing on the hydrophobic membrane. Before illumination, the dispersion was first bubbled with CO_2 for 30 min to achieve a saturated state. Then sample aliquots were taken out in regular time intervals under

illumination. Finally, the concentration of HCOOH was estimated by ion chromatograph (863 Basic IC plus. Metrohm, Switzerland) equipped with a Metrosep A Supp 4-250/4.0 column.

Fluorescent Labelling of FDH

6 mg FDH was first dissolved in 10 ml PBS buffer (pH = 7.4). Then, 1 ml FITC-dimethyl sulfoxide solution (1 mg ml^{-1}) was added to the solution and stirred for 30 min to be dyed. After that, the solution was dialyzed for 1 day to acquire the FITC-labeled FDH solution. All experiments were conducted in the dark condition and the PBS buffer is changed every six hours.

Computational Details

Density functional theory as implemented in the Vienna Ab-initio Simulation Package (VASP) was employed to optimize geometry structures for CN and three different adsorption sites.[1,2] The exchange-correlation interactions were described by the generalized gradient approximation (GGA)[3] in the form of the Perdew-Burke-Ernzerhof functional (PBE)[4]. The vacuum space was set to be more than 20 Å, which was enough to avoid the interaction between periodical images. For optimization of CN, a cut-off energy of 550 eV for plain-wave basis sets was adopted and the convergence threshold was 10^{-6} eV, and 10^{-2} eV/Å for energy and force respectively with cell volume and parameters all freely optimized. For adsorption calculation, a 4*4*1 supercell of CN has been used during the calculation. A cut-off energy of 450 eV for plain-wave basis sets was adopted and the energy convergence threshold was

10^{-6} eV with vdW corrections (DFT-D3 method with Becke-Jonson damping). NCI analysis was carried out employing Multiwfn package[5] and visualized through VMD[6] software. The grid point was set as 0.15 and isosurface value for RDG was 0.30 in this case. Analysis of deformation charge density was carried out through Vesta software[7].

Characterizations

Scanning electron microscopy (SEM) images were recorded on cold field-emission microscopes (Hitachi S-4800 and Regulus-8100) with 15.0 kV accelerating voltage. Transmission electron microscopy (TEM) images were taken on JEM2010 (JEM-F200, Japan) with an acceleration voltage of 200 kV. X-ray diffraction (XRD) was conducted on Ultima IV (Rigaku, Japan) using a nickel-filtered Cu Kα X-ray beam with a scanning angle (2θ) of 5°-80° operating at 40 kV and 40 mA. The scanning rate was set as 20° min^{-1}. Fourier transform infrared (FTIR) spectra measurements were carried out on JASCO4700 recorded from 4000 to 500 cm-1 (Japan). X-ray photoelectron spectroscopy (XPS) was measured on a Thermo ESCALAB 250Xi spectrometer equipped with an Al anode (Al Kα = 1846.6 eV), operated at 15 kV and 10.8 mA. Energy calibration was carried out using the C 1*s* peak of adventitious C at 284.8 eV. UV-vis absorption spectra were carried out on U-3900 (Hitachi, Japan) by using $BaSO_4$ as a reference. The photocurrent response measurement and electrochemical impedance spectra (EIS) were recorded on CHI660 electrochemical workstation (Chenhua, Shanghai, China) equipped with a three-electrode-cell system. The metal loadings of the catalysts were determined with inductively coupled plasma optical emission spectroscopy (ICP-OES) on ICPOES730 (Agilent, Japan). Contact angle was measured

on LSA 60 Surface Analyser (LAUDA Scientific, Germany). The FITC tagged FDH immobilized on the hydrophobic layer was verified using Nikon C2 plus CLSM (Japan). The membrane was exposed under 488 nm, and the emission wavelength was 500-550 nm.

Supporting Table and Figures

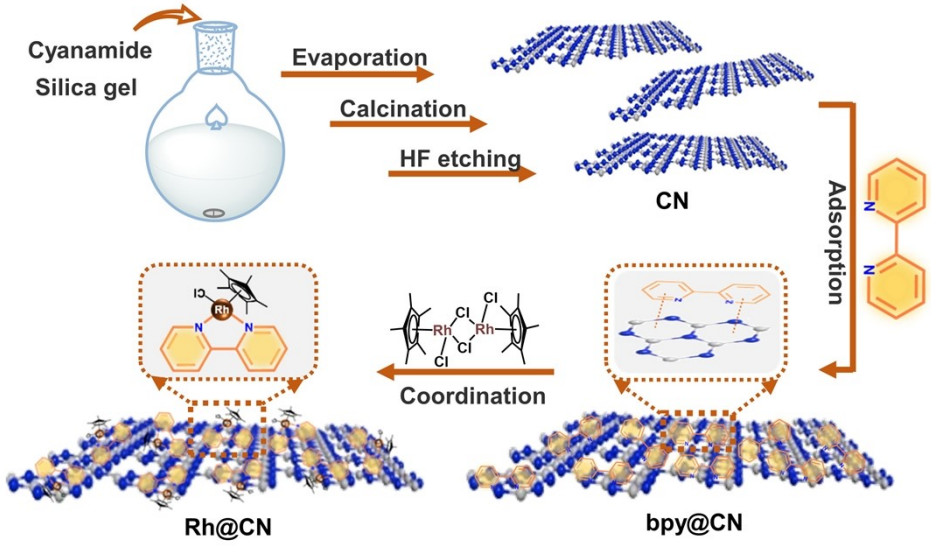

Figure S1. Schematic illustration of the synthetic procedure for Rh@CN.

Figure. S1 displayed the preparation process of Rh@CN. CN was first prepared through a typical pyrolysis and etching procedure using cyanamide as precursor and silica gel as sacrificial template. Then 2,2'-bipyridine, as the most common ligand for the formation of Rh complex, was introduced into CN after impregnation and annealing, giving the intermediate, bpy_{m3}@CN. Further with metal complexation, Rh_{m3}@CN can be obtained successfully.

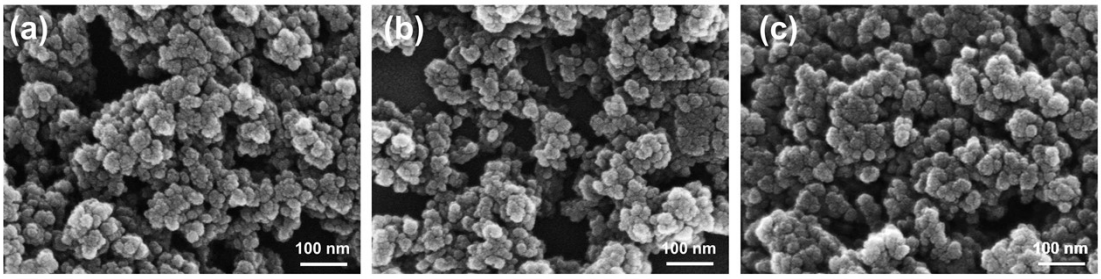

Figure S2. SEM images for CN, bpy_{m3}@CN, and Rh_{m3}@CN.

Figure S2 reveals the morphology of CN, bpy_{m3}@CN, and Rh_{m3}@CN. They all showed granular morphologies.

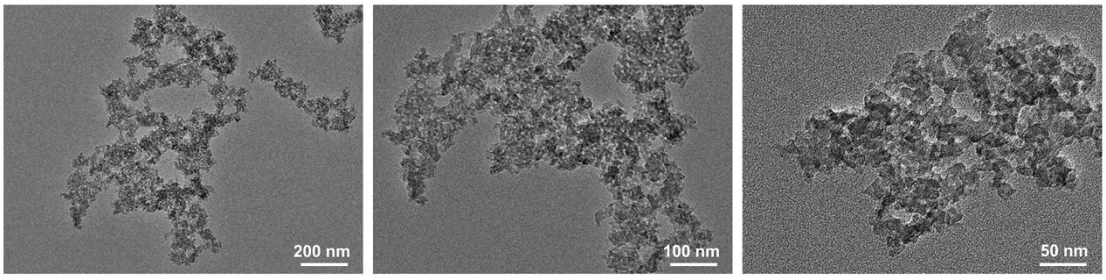

Figure S3. TEM images of Rh_{m3}@CN.

Figure S3 shows the TEM images of Rh_{m3}@PCN. Rh_{m3}@CN features granular structure with aggregates to some degree.

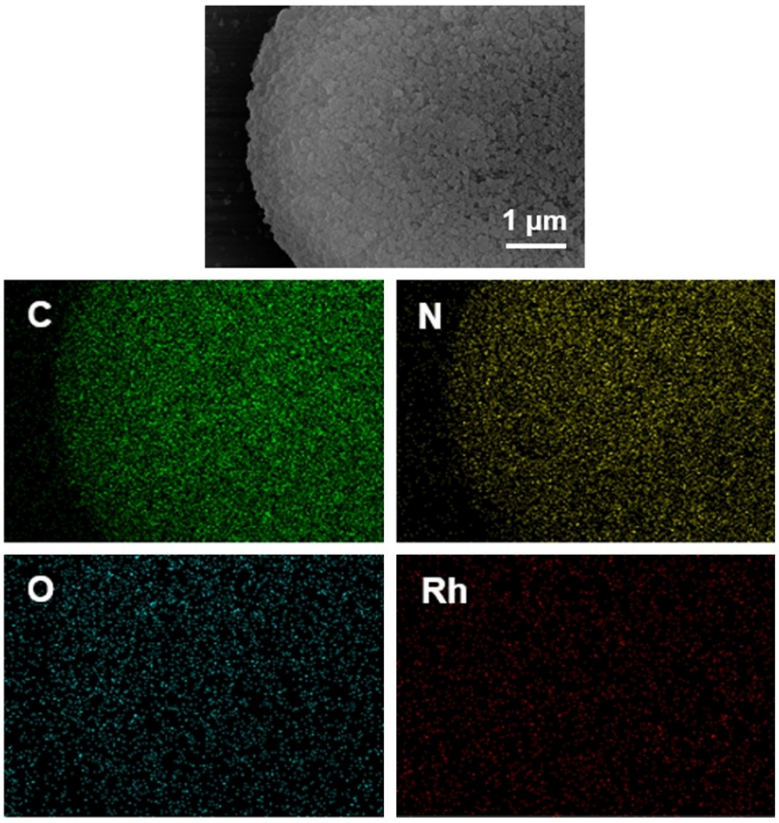

Figure S4. EDS elemental mapping images attached to SEM for Rh_{m3}@CN.

Figure S4 depicted the quite uniform dispersion of C, N, O, and Rh among Rh_{m3}@CN.

But the content of O and Rh were relatively low.

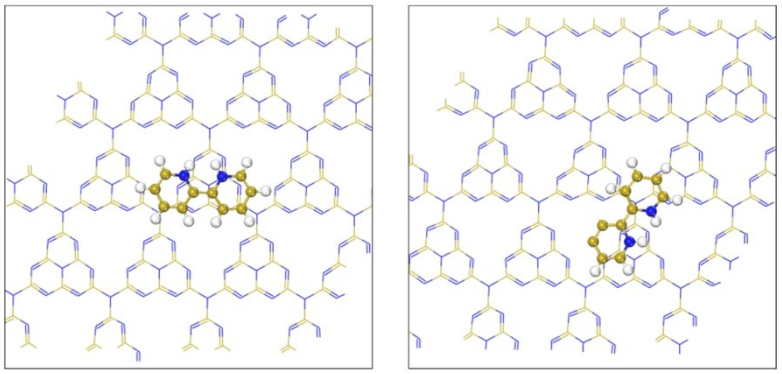

Figure S5. DFT calculations for different absorption models of bpy on the surface of CN and the corresponding adsorption energies.

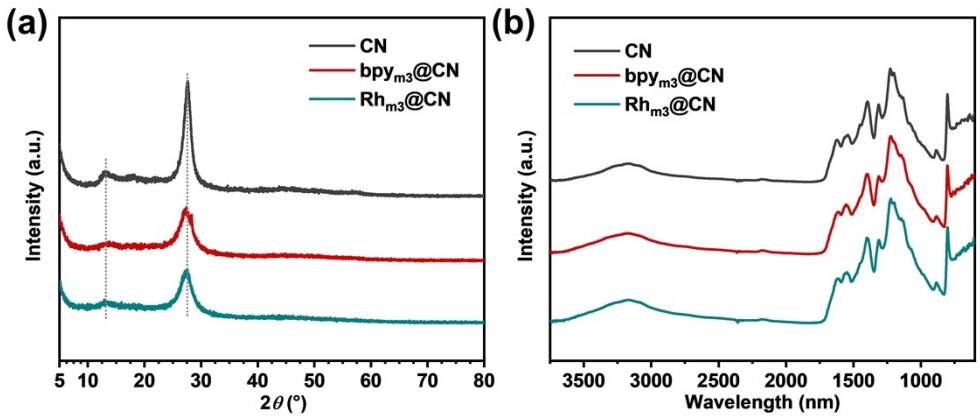

Figure S6. XRD patterns (a) and FTIR spectra (b) for CN, bpy$_{m3}$@CN, and Rh$_{m3}$@CN.

XRD patterns were measured (Figure S6a) to unveil the crystallinity information of CN samples. Two typical diffraction peaks at ~13.2°and ~27.5° were found in the spectra, assigning to the in-plane repeating units of heptazine (100) and the interlayer stacking along the c-axis (002) in CN. FTIR) spectra were used to investigate the chemical structure of the samples (Figure S6b), where only the typical peak patterns of CN frameworks were found. Specifically, the peak at 810 cm^{-1} belongs to the out-of-plane bending mode of heptazine rings, the peaks at 1100-1700 cm^{-1} ascribe to the N-C=N heterocyclic rings, while the peaks at 3000–3500 cm^{-1} correspond to the N-H stretching vibrations.

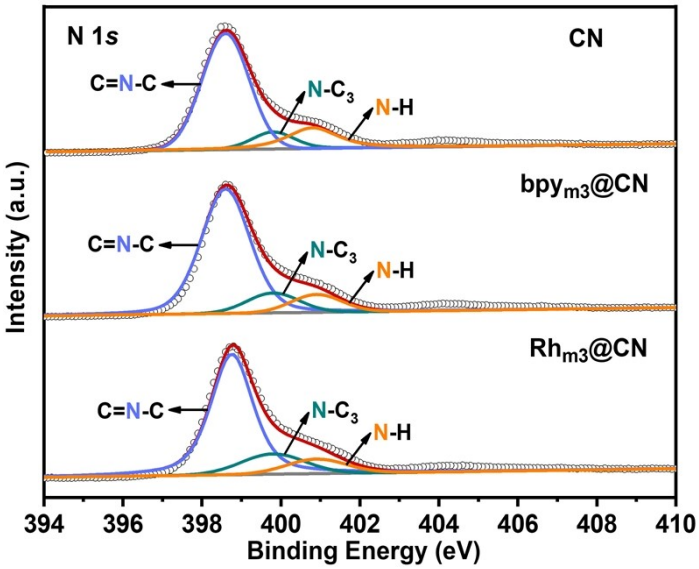

Figure S7. N 1*s* XPS spectra for CN, bpy_{m3}@CN, and Rh_{m3}@CN.

Figure S7 depicted the N 1*s* XPS spectra for the CN samples. They showed similar characteristic peaks located at around 400.9, 399.8, and 398.6 eV, which attributed to the amino groups ($C–NH_x$, x = 1 or 2), tertiary nitrogen $N-(C)_3$, and sp^2-hybridized nitrogen (C–N=C) in tri-s-triazine rings, respectively.

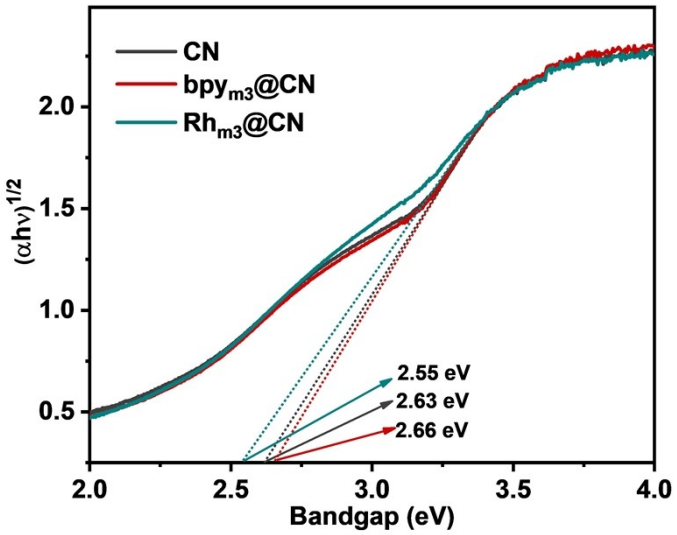

Figure S8. The Tauc plots for CN, bpy$_{m3}$@CN, and Rh$_{m3}$@CN using Kubelka–Munk parameter as a function versus the photon energy.

As determined from the transformed Kubelka–Munk function, the band gaps (E_g) of the three samples were calculated to be 2.55, 2.63, and 2.66 eV, respectively.

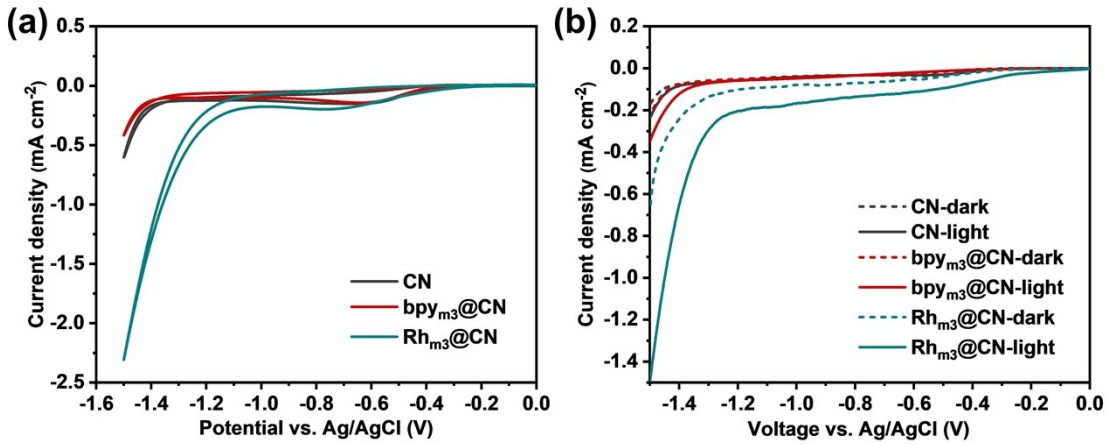

Figure S9. CV curves (a) and LSV (b) curves under light or in dark conditions for CN, bpy_{m3}@CN, and Rh_{m3}@CN.

Photoelectrochemical measurements were conducted to reveal the electron transfer behaviors of CN, bpy_{m3}@CN and Rh_{m3}@CN. The three samples showed similar reduction onset potentials at ~−0.6 V. But Rh_{m3}@CN exhibited a much higher current density at −1.5 V, which was about 5.5 times higher than that of CN with homogeneous Rh complex (Figure S9a). For LSV measurement, the three samples all showed higher current densities under light illumination than those in dark, especially for Rh_{m3}@CN, whose photo-response current increased dramatically, indicating the good light harvesting and response ability of our PCN samples (Figure S9b).

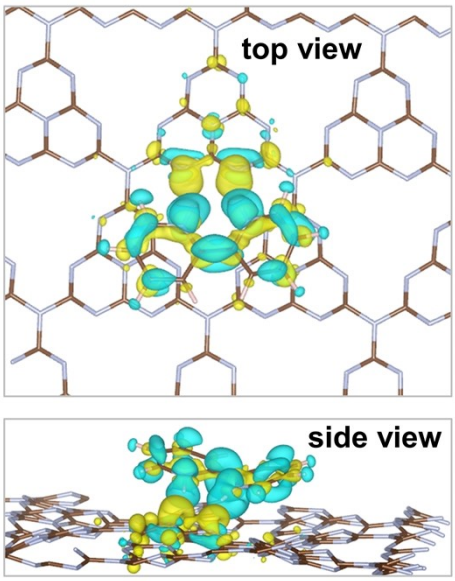

Figure S10. Deformation charge density isosurface of site 2, top view and side view. Color: Yellow indicates positive values, and green indicates negative values.

Analysis of deformation charge density was carried out to explain the interactions between adsorbed bpy molecules and the surface of CN substrate. Electron transfer from pyridinic-N in CN to adsorbed bpy can be seen clearly in Figure S10. Such interaction could separate the electron and hole pairs efficiently, thus facilitating the electron transfer. The special structures of CN should contribute to such phenomenon.

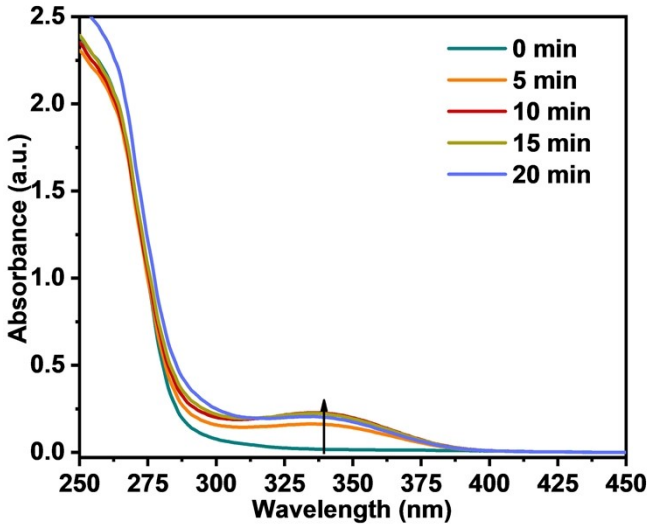

Figure S11. The UV-vis absorbance profile of photocatalytic NADH regeneration catalyzed by Rh_{m3}@CN under light illumination.

Figure S11 is the NADH conversion plot over time during the photocatalytic reaction for Rh_{m3}@CN. In a typical process, sample aliquot was taken in regular time intervals under illumination. Here in ou work, sampling time points were set as 0 min, 5min, 10min, 15min, and 20 min. The change of NADH concentration was determined by measuring the absorption at 340 nm using UV-vis spectrometer. Note that the testing solution was diluted for 10 times before examination. The calculation of conversion was based on the following formula:

NADH conversion (%) = $[(A_1-A_0) \times 10]/6.22 \times 100\%$

where A_0 and A_1 refer to the initial and final absorbance values at 340 nm, respectively. The constant 6.22 results from the absorption coefficient (6220 M^{-1} cm^{-1}) of the absorption peak at 340 nm.

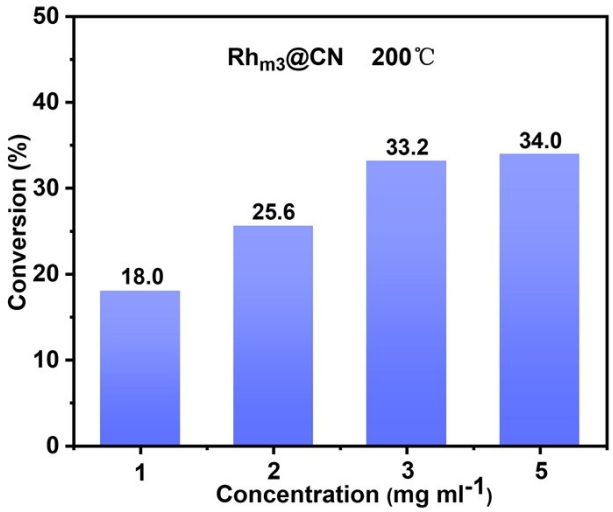

Figure S12. The maximum NADH conversion yield catalyzed by different concentration of Rh_{m3}@CN.

The concentration of Rh_{m3}@CN for photocatalysis was evaluated. With the concentration of 1, 2, 3, and 4 mg ml^{-1}, conversion yields of 18 %, 25.6 %, 3.2 %, and 34.0 % were obtained in 10 min, respectively (Figure S12). For a tradeoff between concentration change versus conversion improvement, 3 mg ml^{-1} was chosen as the optimal concentration.

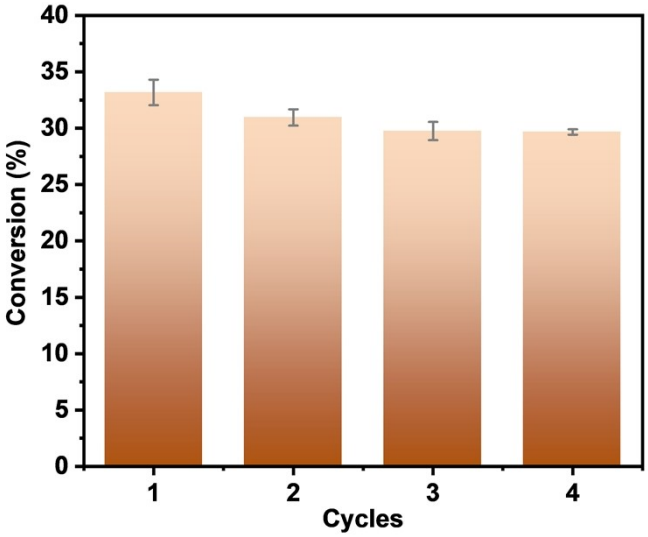

Figure S13. Recycling stability of Rh_{m3}@CN for photocatalytic NADH regeneration.

Rh_{m3}@CN was applied for the photocatalytic NADH regeneration under blue light irradiation (450 nm). The recycling stability of the photocatalyst was evaluated by centrifuging the catalyst from the catalytic system. After washing and drying, the obtained catalysts were re-dispersed into a fresh reaction solution for the next cycle. As shown in Figure S13, the regeneration yield of Rh_{m3}-N-PCN remained ~30% after 4 catalytic cycles.

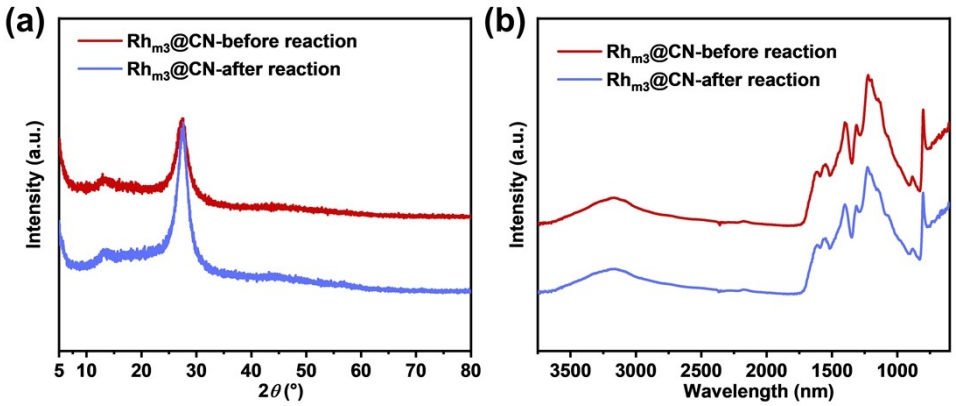

Figure S14. XRD patterns (a), FTIR spectra (b) for Rh_{m3}@CN before and after photocatalysis.

The used photocatalyst was collected by centrifugation from the catalytic system. After washing and drying, the obtained spent Rh_{m3}@CN was applied for XRD and FTIR measurements. As shown in Figure S14a, both the fresh and used samples exhibited XRD peak positions at ~13.2° and 27.5°. Similarly, little changes were found in the structural composition in the FTIR spectra for Rh_{m3}@CN before and after photocatalysis (Figure S14b).

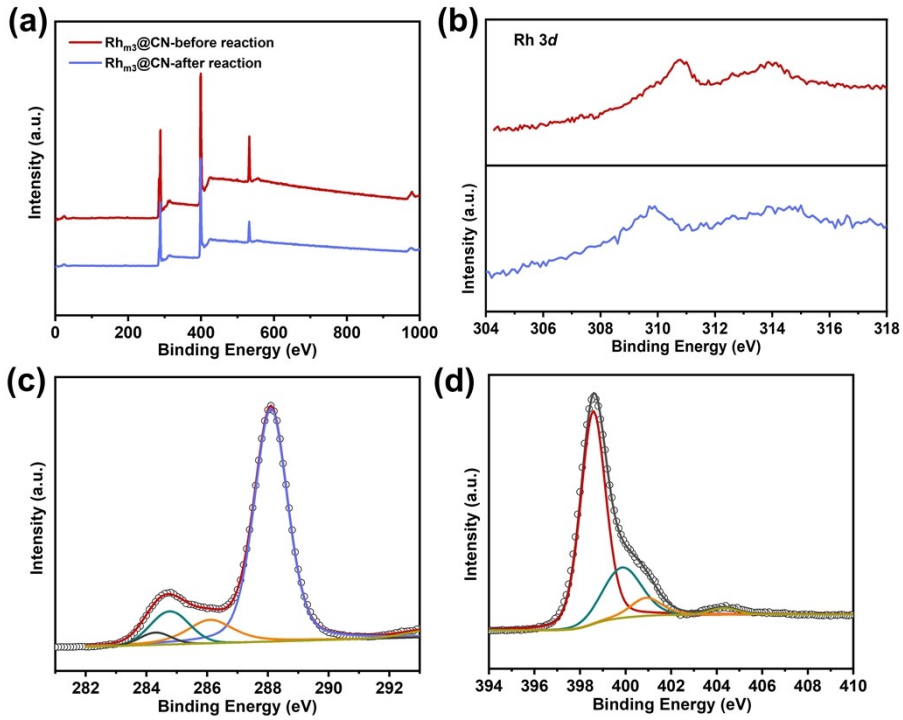

Figure S15. XPS survey spectra (a), and the high-resolution Rh 3*d* spectra (b) for fresh and spent Rh_{m3}@CN, respectively. High-resolution C 1*s* spectrum (c) and N1*s* spectrum (d) for spent Rh_{m3}@CN.

As can be seen from Figure S15a, both the fresh and spent Rh_{m3}@CN showed peaks for C, N, O, and Rh in the survey spectra. In detail, their high-resolution Rh 3*d* peaks could both be deconvoluted into peaks with binding energies of 314.2 eV and 309.7 eV, which corresponding to Rh $3d_{2/3}$ and Rh $3d_{5/2}$, respectively (Figure S15b). For the high-resolution C 1*s* species, peaks attributing to pristine PCN (~288.2, 286.3, 284.8 eV) as well as the bpy molecule (~284.3 eV) all maintained after photocatalysis (Figure S15c). Similarly, slight difference could be found in the N 1*s* spectra for sample before and after reaction (Figure S15d). The results indicated the quite good stability of Rh_{m3}@CN for photocatalysis.

Reference

1. G. Kresse and J. Furthmuller, Phys. Rev. B, 1996, 54, 11169-11186.
2. G. Kresse and J. Furthmuller, Comput. Mater. Sci., 1996, 6, 15-50.
3. J. P. Perdew, K. Burke and M. Ernzerhof, Phys. Rev. Lett., 1996, 77, 3865-3868.
4. B. Zhu, K.X. Wang, H.L. Gao et al., ChemPhysChem, 2021, 22, 1–10.
5. H.D. Hu, L.L. Chen, Appl. Phys., 2014, 4, 155-161.
6. W. Humphrey, A. Dalke and Schulten, K., J. Molec. Graphics, 1996, 14, 33-38.
7. K. Momma and F. Izumi, J. Appl. Crystallogr., 2008, 41, 653-658.